Filament instability and rotational tissue anisotropy: A numerical study using detailed cardiac models

Wouter-Jan Rappel[a]

Department of Physics, University of California, San Diego, La Jolla, California 92093

The role of cardiac tissue anisotropy in the breakup of vortex filaments is studied using two detailed cardiac models. In the Beeler–Reuter model, modified to produce stable spiral waves in two dimensions, we find that anisotropy can destabilize a vortex filament in a parallelepipedal slab of tissue. The mechanisms of the instability are similar to the ones reported in previous work on a simplified cardiac model by Fenton and Karma [Chaos **8**, 20 (1998)]. In the Luo–Rudy model, also modified to produce stable spiral waves in two dimensions, we find that anisotropy does not destabilize filaments. A possible explanation for this model-dependent behavior based on spiral tip trajectories is offered. © *2001 American Institute of Physics.* [DOI: 10.1063/1.1338128]

Ventricular fibrillation (VF), characterized by incoherent electrical activity of the heart, is the leading cause of sudden death in the industrialized world. Despite intense research efforts in the past decades, the mechanisms involved in the initiation and maintenance of VF remain largely unknown. A clear understanding of these mechanisms is essential for the development of new devices and pharmaceutical strategies in the treatment of VF. One possible mechanism responsible for the generation of VF is tissue anisotropy, which is inherently present in cardiac tissue. This anisotropy can destabilize scroll waves, thought to be precursors of VF. Here, we investigate the effect of rotational tissue anisotropy on the stability of scroll waves and their filaments using two detailed cardiac models: the Beeler−Reuter (BR) model and the Luo−Rudy (LR) model. We find that the two models lead to dramatically different stability results. The BR model is found to be able to destabilize scroll waves which can lead to fibrillatory behavior. Scroll waves in the LR model, on the other hand, remain stable, even for thick, highly anisotropic slabs of tissue. It is argued that this surprising result might be due to the different spiral tip trajectories in the two models.

I. INTRODUCTION

Numerical modeling efforts of electrical wave propagation in the heart have seen a surge of interest recently.[1] This surge can be attributed to several reasons. Among them are the dramatic increase in computational power over the last several decades that has led to faster computers that can handle more complex and computationally intensive problems. In addition, the description of the many membrane channels involved in the electrical activity of cardiac cells has improved substantially, leading to detailed cardiac models. Finally, recent research has linked certain diseases that lead to a larger predisposition for cardiac arrhythmias to spe-

cific defects in channels. For example, the long QT syndrome, which is characterized by a prolonged ventricular repolarization and which manifests itself as an abnormally long QT interval in the ECG, has been found to be associated with defects in several channels. These defects can be congenital, idiopathic, or acquired.[2] Numerical attempts at clarifying the roles of the affected channels in the diseases in conjuncture with clinical investigations raise the hope of finding effective pharmacological treatments.

Despite the recent flurry of activity in the field, there remain numerous unanswered questions. In particular, it is still not known what causes the onset of fibrillation, a fatal cardiac arrhythmia during which the heart ceases to contract coherently. Even more pointedly, the exact underlying mechanisms of fibrillation are not known. It is generally believed that reentry phenomena, which occur when the propagation of the electric wave is blocked in a direction causing the wave front to curl and reenter the previously excited tissue, play an important role in fibrillation. However, it is not clear if fibrillation is due to many simultaneous reentry events[3,4] or if it is due to a limited number of fast moving reentry events.[5]

In this paper we will investigate tissue anisotropy as a possible cause for fibrillatory behavior. Tissue anisotropy is inherently present in mammal hearts and has been shown to play an important role in the breakup of three dimensional (3D) scroll waves in recent numerical work.[6–8] The studies utilized, to various degrees, simplified models for cardiac propagation. The aim of this paper is to investigate the effect of tissue anisotropy in more detailed cardiac models. To this end, we use two cardiac models: the Beeler–Reuter (BR) model[9] and the original Luo–Rudy (LR) model.[10] The choice of these models was motivated by the necessity of a model that is still within reach of current computers, particularly in three dimensions, and of a model that is sufficiently close to reality.

This paper is organized as follows. In Sec. II we describe the anatomy of heart walls. In Sec. III we discuss previous work on anisotropy mediated instabilities and in Sec. IV we present the numerical details of our work. In Sec. V we show

[a]Electronic mail: rappel@herbie.ucsd.edu
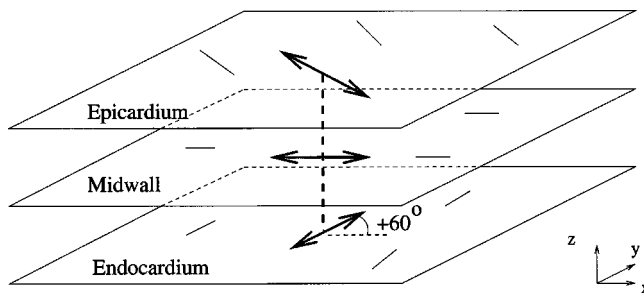
© 2001 American Institute of Physics

FIG. 1. The three-dimensional parallelepipedal slab geometry with rotating anisotropy used in this study.

simulations in two dimensions (2D) and discuss the modifications to the BR and LR model that are made in this work. In Sec. VI we discuss the effect of anisotropy on the stability of vortex filaments in the BR and LR models and Sec. VII contains the conclusion.

II. TISSUE ANISOTROPY

The actual morphology of the ventricular wall is complicated; the myocardium displays a laminar structure with cells stacked in sheets of varying orientation.[11,12] To simplify and facilitate the implementation of anisotropy the morphology of previous modeling studies will be used[6,7] where the myocardial cells are arranged in sheets that lay parallel to the epi- (outside wall of the heart) and endocardium (inside wall of the heart).[13] Myocardial cells can be viewed as roughly rod-shaped with an elliptical cross section with a long axis of ≈ 100 μm and a cross-sectional diameter of ≈ 10–20 μm. As a consequence of the rodlike shape of the cells, the propagation speed of electrical waves is roughly 2–3 times larger along the fiber axis than perpendicular to it. The fiber axis of the cells is identical within each sheet and rotates continuously as one traverses the ventricular wall from epi- to endocardium. The rate at which the fiber angle rotates is nearly constant throughout the heart and a typical total rotation of the human left ventricular wall (1–2 cm) is 120°. A schematic picture of the geometry used in this study is displayed in Fig. 1.

III. PREVIOUS RESEARCH

Early numerical work in cardiac models has found a variety of mechanisms that can destabilize a propagating planar wave. Among these mechanisms are the inclusion of one or more heterogeneities in the ''tissue'' and the application of a premature stimulus in the so-called vulnerable window of the tissue. The ensuing spatiotemporal pattern after the initial instability is typically a spiral wave, a generic state in models of excitable media.[14] Experimentally, there is ample evidence of the existence of spiral waves and they have been found in cardiac tissue slices of a variety of species including rabbits,[5,15] sheep,[16] and dogs.[17]

The occurrence of a single spiral wave leads to a state of high frequency with, depending on the tip trajectory of the spiral, a variable amount of coherency. This state is believed to correspond clinically to ventricular tachycardia (VT), which is manifested by an elevated heart beat in patients.

During ventricular fibrillation (VF), however, the dynamics of the heart is completely incoherent. A possible explanation for the transition between VT and VF is a secondary instability which destabilizes the spiral wave and leads to multiple centers of activity. Such an instability was found in computer models, given the right set of parameters.[18] In experiments in thin tissue, however, spiral waves were *not* found to be unstable.[19,20] In fact, it was found that a minimum thickness, approximately 3–4 mm, of the tissue was needed to observe VF. This suggests that the degeneration of VT into VF is a 3D phenomenon. The 3D equivalent of a spiral can be produced by taking a 2D spiral and stacking it in a third dimension. The thus formed scroll wave or vortex rotates around a singularity line called the filament. Based on the experiments that showed that a minimum thickness was necessary to induce VF, it has been postulated that a vortex filament instability plays a crucial role in the onset of VF.[21]

One mechanism that can be responsible for a filament instability was recently investigated numerically. The studies utilized simplified models for cardiac propagation. Panfilov and Keener[6] used the FitzHugh–Nagumo model while Fenton and Karma (FK)[7,8] used a three-variable model in which parameters can be adjusted to replicate a desired restitution curve, to be defined in Sec. IV. Both studies found that the presence of tissue anisotropy can destabilize a scroll wave with a filament extending from the endo- to epicardium. FK performed a thorough quantitative study and found that a filament breaks up into multiple pieces above a critical thickness which decreases with increasing degree of anisotropy. In the absence of anisotropy the filament remains stable even for thick (>1 cm) tissue slabs. The instability was found to be produced by a buildup of twist of the vortex filament. This twist is nonhomogeneously distributed and areas of localized twist, termed twistons by FK, can travel along the filament. Two dominant mechanisms for the formation of filaments were identified by FK: (1) a curved intramural filament collides with a boundary, creating a closed half ring and (2) a half ring that expands and collides with a boundary, generating two intramural filaments (see also Fig. 5).

As mentioned previously, these studies utilized simplified ionic models for electrical wave propagation. It needs to be checked if the same mechanisms are also present in more detailed models. For example, even though the restitution curve in Ref. 7 is identical to the one of the full BR model, the three variable model does not necessarily duplicate other features. Spiral wave period, wavelengths, core sizes, and filament trajectories are not necessarily the same. It is therefore worthwhile to investigate the effect of tissue behavior in more detailed models.

IV. NUMERICAL DETAILS

The equation describing the membrane potential can be written as

$$\frac{\partial V}{\partial t} = \nabla \cdot \tilde{D} \nabla V - \frac{I_{\text{ion}}}{C_m}, \qquad (1)$$

where V (mV) is the membrane potential, C_m (μF cm^{-2}) is the membrane capacitance, ∇ is the gradient operator, and

I_{ion} (μA cm^{-2}) is the total ionic current flowing through the cardiac cell membrane. $\tilde{D}$ is a 3×3 matrix which reflects the different propagation speeds along and transverse to the fiber orientation and can be written as

$$\tilde{D} = \frac{\tilde{\sigma}}{S_v C_m} = \begin{bmatrix} D_{11} & D_{12} & 0 \\ D_{21} & D_{22} & 0 \\ 0 & 0 & D_\perp \end{bmatrix},$$

where $\tilde{\sigma}$ is the conductivity tensor and S_v (cm^{-1}) is the surface to volume ratio. The matrix elements are given by

$$D_{11} = D_\parallel \cos^2 \theta(z) + D_\perp \sin^2 \theta(z), \qquad (2)$$

$$D_{22} = D_\parallel \sin^2 \theta(z) + D_\perp \cos^2 \theta(z), \qquad (3)$$

$$D_{12} = D_{12} = (D_\parallel - D_\perp) \cos \theta(z) \sin \theta(z). \qquad (4)$$

Here, $D_\parallel$ is the diffusion constant for propagation parallel to the fiber, $D_\perp$ is the diffusion constant for propagation perpendicular to the fibers (taken to be the same in both perpendicular directions), and $\theta(z)$ is the angle between the x axis and the fiber orientation:

$$\theta(z) = -\theta_0 + z\gamma. \qquad (5)$$

θ_0, the angle between the fiber axis of the bottom face of the slab, taken to be the endocardium, and the x axis was set to be 60°, while γ, the rotation rate per length and the thickness of the wall, L_z, were varied. Values for the constants used in this paper are: $C_m = 1$ μF cm^{-2} and $S_v = 5000$ cm^{-1}, $D_\parallel = 1$ cm^2/s and $D_\perp = 0.2$ cm^2/s. Zero flux boundary conditions are implemented by imposing

$$\hat{n} \cdot \tilde{D} \nabla V = 0, \qquad (6)$$

where $\hat{n}$ is the normal vector to the boundaries of the computational domain.

The main difference between existing cardiac models is the description of I_{ion}, which describes the working of the membrane channels that regulate the influx and efflux of ions. Trying to incorporate all known channels in a computer model is currently not feasible. Such a model would be too computationally intensive for current computers. In addition, some channels are quantitatively poorly described and incorporating them in detailed models can lead to unphysical results. For example, recently developed models such as a later version of the LR model[22] and one by Winslow and collaborators[23] are not always stable under fast or prolonged pacing.[24] It is therefore essential to maintain a sensible balance between accuracy and computational requirements in choosing I_{ion}.

Both the BR and the LR models consist of four currents (fast inward sodium, slow inward calcium, time-dependent potassium, and time-independent potassium) and their gating variables, with Hodgkin–Huxley type dynamics,[25] as well as an equation for the calcium uptake by the cell. The LR model is more recent than the BR model and contains a different description of the fast inward sodium current and the time-dependent potassium current and a more complete description of the time-independent potassium current. For explicit expressions for the currents and gating variables ap-

pearing in (1) we refer to Ref. 9 for the BR model and Ref. 10 for the LR model, respectively. One remark has to be made concerning the LR model. As was already pointed out in Ref. 26, the expressions appearing in the original paper of Luo and Rudy do not reproduce all the results of that paper. For this study, we have taken the exact expressions as they appear in Ref. 10.

Several different methods of integration can be used to solve the governing equations numerically. An implicit method has the advantage that it is stable for much larger time steps than an explicit method. Unfortunately, the time constants of several gates, and the activation gate of the Na current in particular, are very small. The resulting stiffness of the problem puts a severe constraint on the allowed time step, nullifying the advantage of using an implicit method. In fact, we found that for the space discretization used mostly in this paper ($\Delta x = 0.25$ mm) a time step of $\Delta t = 0.025$ ms was needed to resolve the planar wave speed in the implicit method to within 5%. For this particular time step, spatial discretization, and method of calculating derivatives (standard center differences) the explicit forward Euler method is stable and is accurate at about the same 5% level. Therefore, we have chosen an explicit forward Euler method as our method of integration. An additional advantage of an explicit method is the relative ease with which it can be parallelized. Part of the simulations reported here were performed on a massively parallel Cray T3E. In summary, the simulations reported here were performed with a spatial discretization of $\Delta x = 0.25$ mm and a time step of $\Delta t = 0.025$ ms except for the runs with a rotation rate of 24°/mm for which we decreased the spatial discretization to $\Delta x = 0.125$ mm and the time step to $\Delta t = 0.005$ ms.

To speed up the calculation we have made extensive use of look-up tables. The activation and inactivation variables $y_i(t)$ that are needed to calculate I_{ion} were evaluated at $t + \Delta t$ using

$$y_i(t+\Delta t) = y_i(\infty) - [y_i(\infty) - y_i(t)] e^{-\Delta t/\tau_i}, \qquad (7)$$

where $y_i(\infty)$ and τ_i are both function of V and are, respectively, the asymptotic value of y_i and the time constant of y_i. Both $y_i(\infty)$ and τ_i as well as the exponential terms were tabulated in increments of 0.1 mV. The actual values used for each time step were obtained by linearly interpolating between the entries in the table. We have verified that the use of look-up tables did not result in an appreciable loss of accuracy (error in plane wave propagation $<$1%), while it led to a gain in speed of approximately 20.

An important characterization of cardiac tissue and cardiac models is the action potential duration (APD) and conduction velocity (CV) restitution curves. These curves relate, respectively, the APD and the CV to the diastolic interval (DI), the recovery time. Since reentry involves reexcitation of recovered tissue, these curves are important factors in the dynamics of reentry patterns.

In Figs. 2(a) and 2(b) we have plotted the APD and the CV restitution curve, respectively. The curves were calculated using a cable of 100 elements, paced at element 1, which was located at one end of the cable. The front and back of the waves were defined to be at -50 mV (roughly
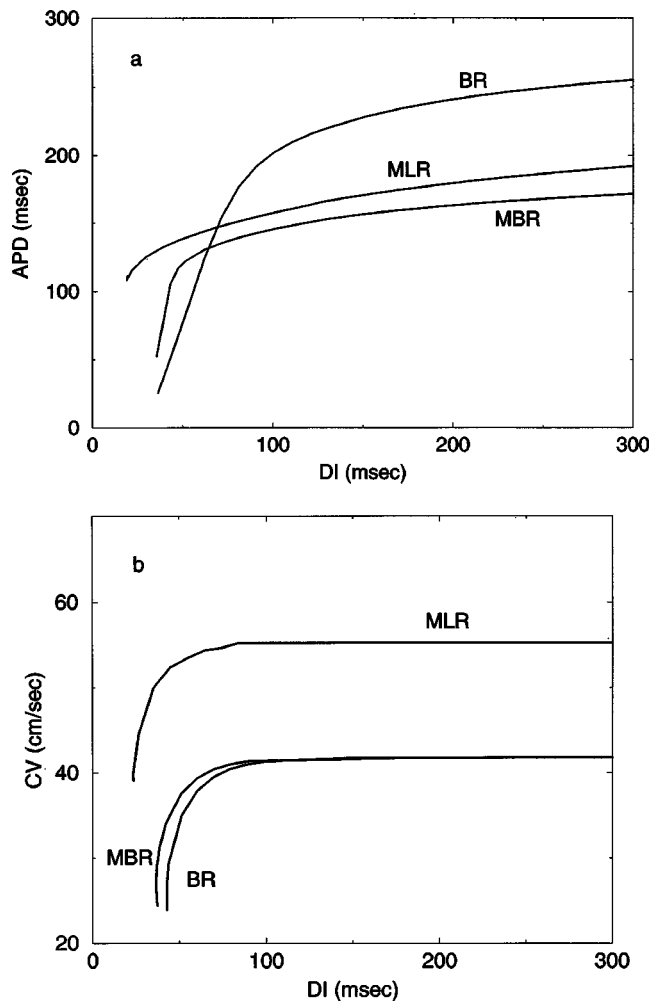
FIG. 2. The APD restitution curve (a) and the CV restitution curve for the original BR model (BR), the BR model with a speed-up factor of 2 for I_{si} (MBR), and the LR model with a speed-up factor of 3 for I_{si} (MLR).
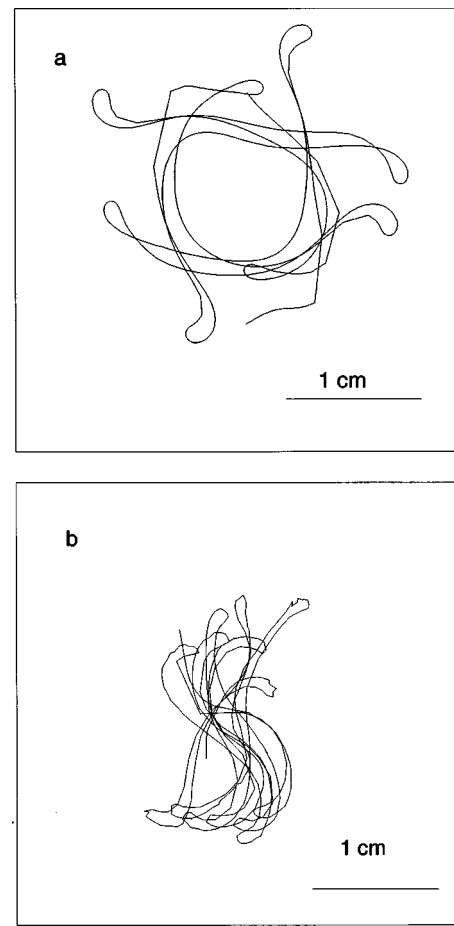
FIG. 3. Typical spiral wave tip trajectories for the BR model with a speed-up factor of 2 for I_{si} (a) and for the LR model with a speed-up factor of 3 for I_{si} (b). The spiral wave in this geometry was produced by the familiar broken wave front procedure. A plane activation wave front that has propagated through most of the tissue is cut in half and allowed to continue its propagation after the potential in the region below the cut is set to zero. The wave front curves and reenters the region which is set to zero and forms a spiral.

80% repolarization) and the APD and DI were calculated at element 20. The velocity was determined by calculating the front speed between elements 10 and 20. The pacing (duration 1 ms, strength 300 μA cm^{-2}) was slowly and progressively increased until it failed to initiate an action potential. We have plotted results for both the modified BR model (MBR) and the modified LR model (MLR). Both models were modified by speeding up the slow inward calcium current, I_{si}, with a factor of 2 and 3, respectively. The reasons for choosing these calcium current speed-ups are explained in Sec. V. For reference, we have also plotted the restitution curves for the original BR model. As is well known, Fig. 2 illustrates clearly that the APD restitution curve of the BR model is much steeper than the APD restitution curve of the LR model.

V. 2D RESULTS

Before we describe our results in 3D it is worthwhile to examine the behavior of spirals in 2D where the tissue anisotropy can always be removed by proper rescaling of the equations. As was previously reported, 2D spirals in the BR model are intrinsically subject to spiral wave breakup.[27] In

Ref. 27 it was also shown that speeding-up the slow inward calcium current, I_{si}, removes this instability. In this paper we choose a speed-up of 2.

There are several way to calculate the tip position. The method employed by FK,[7] calculates the point along a line of constant V ($V = -30$ mV in this paper) where the normal velocity vanishes. The advantage of this method is that it can calculated easily during the simulation. However, as will be explained in the following, this method does not work well for the LR model. Therefore, we used an alternative way to find spiral tip positions in 2D and in slices of 3D geometries. It consists of finding the intersection of a line of constant V ($V = -30$ mV in this paper) and a line of constant value of the inactivation gate variable h for the sodium channel ($h = 0.2$ in this paper).[28] We employed a cubic smoothing spline to both these lines and occasional multiple intersections were resolved manually. A typical spiral tip trajectory in the isotropic BR model with $D_{\parallel} = D_{\perp} = 1$ cm^2/s is plotted in Fig. 3(a).

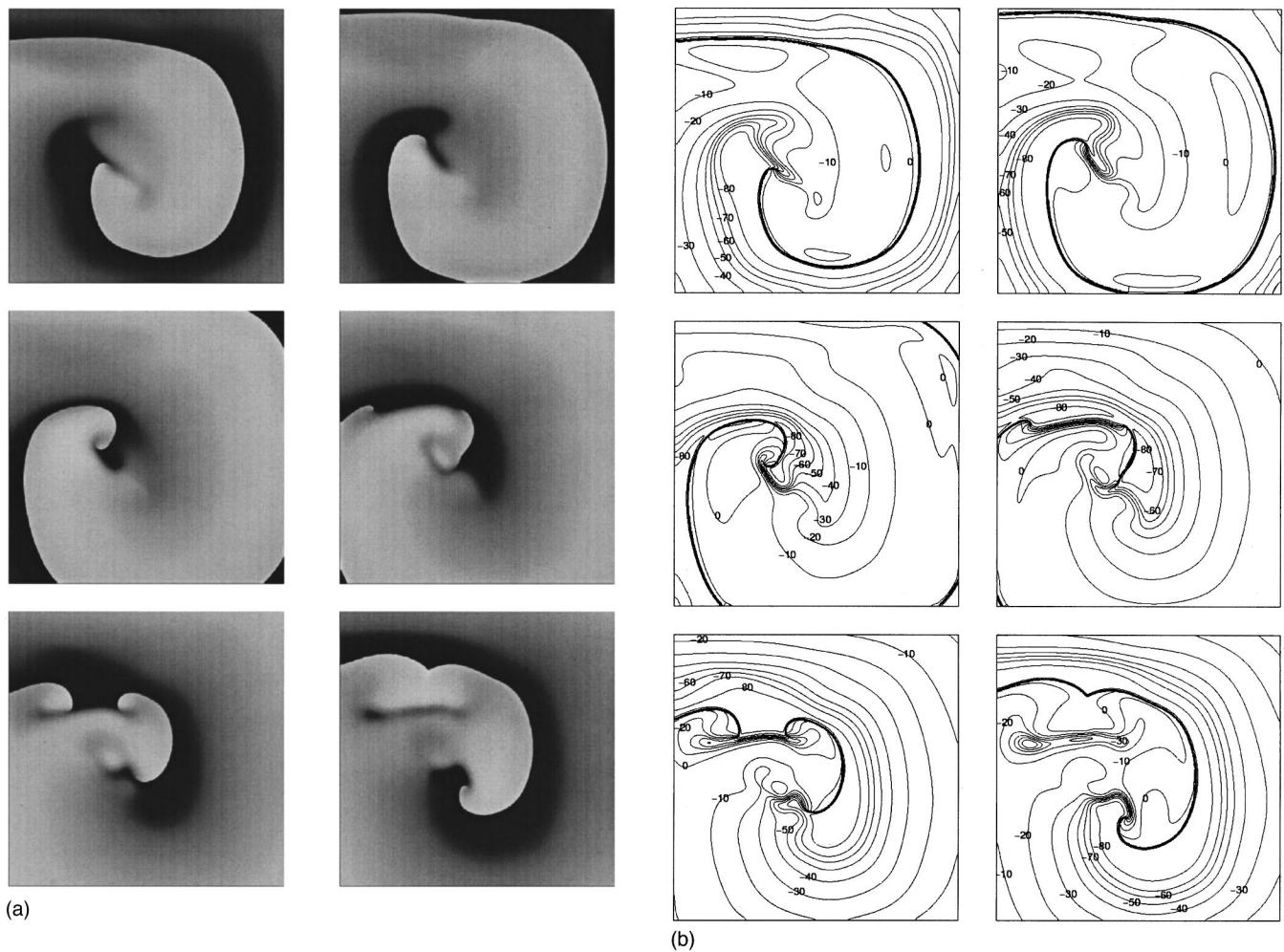Spirals in the unmodified LR model are also prone to spiral wave breakup. Perhaps this is not surprising since the

FIG. 4. Spiral waves in the modified LR model with a speed-up factor of 2.6 for I_{si}. The membrane potential is shown in a gray-scale plot with white corresponding to maximum depolarization and black corresponding to maximum repolarization. The plots are 2.5 ms apart, with the upper left-hand picture being the earliest and the lower right being the latest. Contour plots of the membrane potential ranging from −80 to 10 mV in steps of 10 mV are shown in (b).

description of the I_{si} is essentially identical to the one in the BR model. For this paper, we have chosen to adopt the same modification as used for the BR model, namely a speed-up of I_{si}. We found that spirals become stable when the speed-up factor was larger that 2.8. To illustrate the mechanism for the 2D spiral-wave breakup in the LR model we show in Fig. 4(a) a typical sequence of a spiral-wave breakup for a speed-up of 2.6. The gray-scale represents the membrane potential values with white corresponding to maximum depolarization and black corresponding to maximum repolarization. Figure 4(b) shows the isocontour plots of V in increments of 10 mV starting at −80 mV and clearly illustrates that the breakup is due to a region of slow repolarization. This breakup mechanism is identical to the one in the BR model and was dubbed second repolarization waves in Ref. 27. For smaller values of the speed-up factor the breakup becomes more pronounced and leads to multiple spirals in the computational box.

In Fig. 3(b) we show a typical spiral tip trajectory for a speed-up of 3, the value used in this study. A comparison between Figs. 3(a) and 3(b) reveals that the LR model displays a qualitatively different tip trajectory than the BR model. In the LR model, the core is linear and the trajectory before and after a turn rarely cross. In the BR model, on the other hand, the core is less linear, the turns are smoother, the trajectory before and after typically cross shortly after a turn, and the overall scale of the meandering patterns is larger. We will argue in Sec. VI that the difference in tip trajectories has an important effect on the destabilization of vortex filaments.

The features of the tip trajectories in the LR model are responsible for the failure of the FK tip position algorithm. The spiral tip travels along a conduction block that is the result from the repolarizing waveback. Since this line is nearly perfectly straight directly following a turn, the FK algorithm does not find a point with vanishing normal velocity along lines of constant V on the wave front. Instead, it finds a point with vanishing normal velocity along lines of constant V on the waveback.

VI. 3D RESULTS

Using the modified version of the BR and LR models described previously we investigated the effect of anisotropy on the stability of a vortex filament. The simulations were
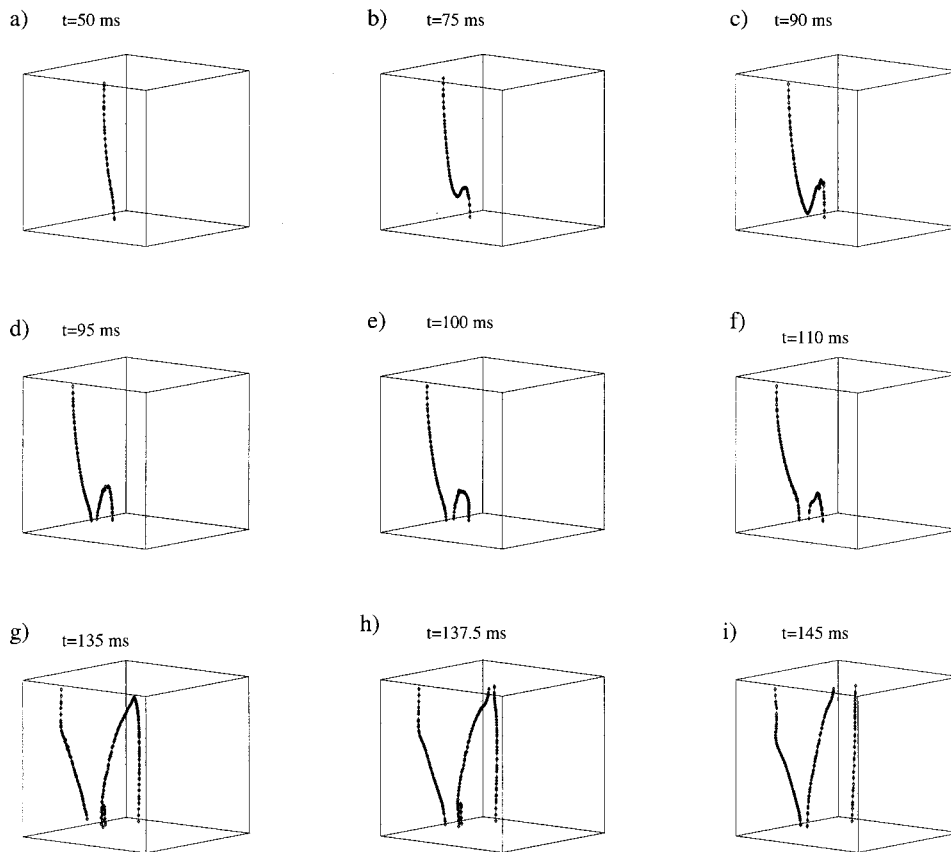
a)   t=50 ms

b)   t=75 ms

c)   t=90 ms

d)   t=95 ms

e)   t=100 ms

f)   t=110 ms

FIG. 5. Illustration of the mechanisms of early filament breakup. The slab has a thickness of $L_z = 9$ mm with a rotation rate $\gamma = 12°$/mm. For clarification purposes in all figures showing filaments, the z direction is expanded.

g)   t=135 ms

h)   t=137.5 ms

i)   t=145 ms

performed in a $200 \times 200 \times N_z$ slab corresponding to a domain with physical dimensions $5 \times 5 \times 0.025 N_z$ cm. As initial condition we used a 2D spiral, obtained from the 2D BR model which was modified by speeding up I_{si}, stacked in the z direction. Note that this modification was necessary to ensure stable filaments in the absence of any perturbation. This created a straight initial element that is perpendicular to the

epi- and endocardium. The angle between the fiber axis of the bottom face of the slab and the x axis was taken to be $60°$.

A. BR model

Our numerical results for the BR model are largely similar to the ones obtained by FK with their simplified model. In

t=0 ms
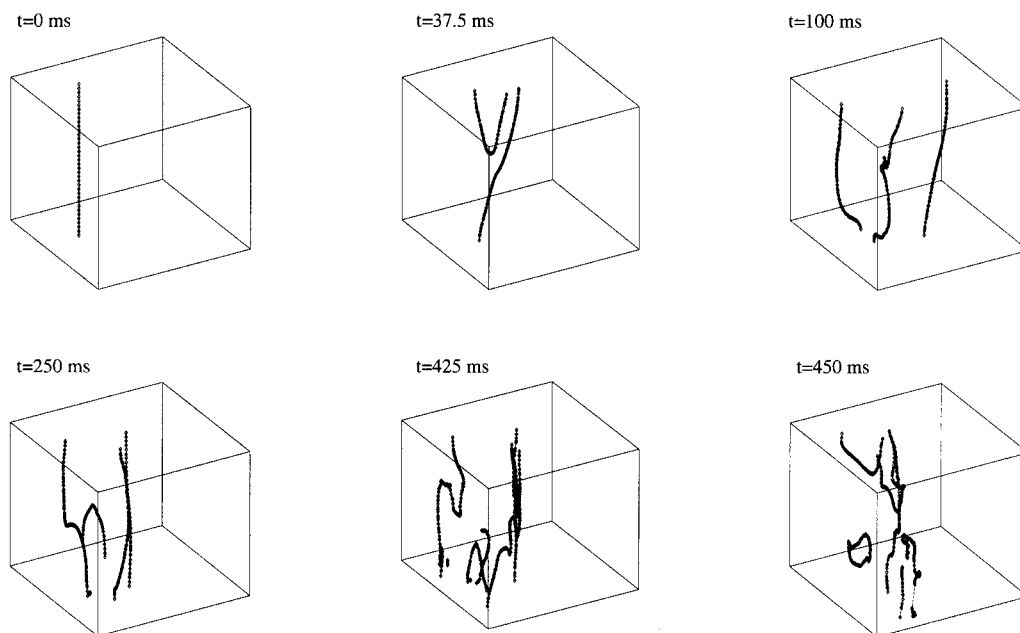
t=37.5 ms

t=100 ms

t=250 ms

t=425 ms

t=450 ms

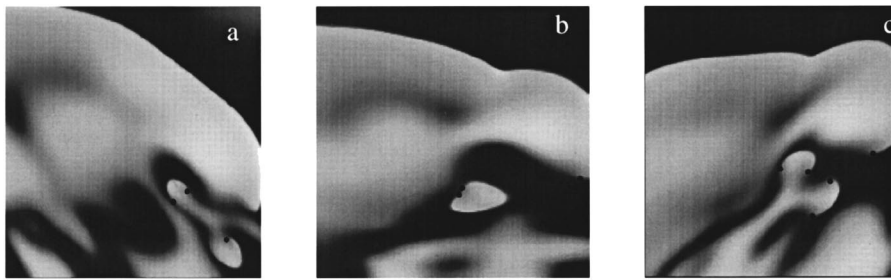FIG. 6. Breakup of filaments for a slab with $L_z = 12$ mm and $\gamma = 12°$/mm.

FIG. 7. Gray-scale plots of the membrane potential for a slab with $L_z = 12$ mm and $\gamma = 12°/$mm during fully developed irregular activity for the endocardium (a), epicardium (b), and the midwall, a plane parallel to the endocardium and midway between the endo- and epicardium. The closed circles correspond to the location of the filament.

particular, in the BR model we find that destabilization of the vortex filament can only occur above a critical thickness, which decreases for increasing fiber rotation rates. The dominant mechanisms for filament creation in the BR model are illustrated in Fig. 5 for a slab with a thickness $L_z = 9$ mm and a rotation rate $\gamma = 12°/$mm. In frames a–f, the filament buckles and breaks apart when the curved part touches the lower boundary. In frames g–i, the half ring created after a collision with the boundary expands and forms two separate filaments when it reaches a boundary. As time progresses, the activity becomes more irregular and multiple filaments appear. An example of this fibrillatorylike behavior can be seen in Fig. 6. The filaments in these and following figures were calculated as described in Ref. 7. To illustrate the irregular activity further we plot in Fig. 7 the membrane potential in three slices parallel to the endocardium. The gray plots show clearly that the electrical activity has become disorganized. We have verified that a buildup of twist is responsible for the destabilization of the filament. Furthermore, as was discovered by FK, the twist is not uniformly distributed along the filament. Instead, it is concentrated in a finite area which propagates along the filament.

Our results are summarized in Fig. 8, where we have plotted the outcome of our numerical runs in rotation rate versus wall thickness space. Runs that produced irregular,

VF-like behavior, are indicated by closed circles, runs in which occasionally additional filaments are created are plotted as gray squares, and runs in which the filament remains a line are plotted as open circles. The solid line is the boundary between the region in parameter space where our results predict filament breakup and VF and the region where filaments are stable, corresponding to VT. For comparison, the dashed line is the same boundary found by FK. Qualitatively, our results and the results of FK agree well.

B. LR model

We repeated the simulations described in Sec. VI A using the LR model. The model was modified by speeding-up the slow inward current by a factor of 3. Unlike the BR model, the LR model was *not* found to destabilize a vortex filament, even for $L_z = 12$ mm and $\gamma = 24°/$mm. Even though the FK algorithm to calculate the spiral tip and filament position cannot provide quantitatively accurate results, especially directly following a turn, it can still offer qualitative insight. Using this algorithm we found that occasional shedding of a vortex was present but no sustained unorganized behavior could be observed. In a separate set of numerical experiments, we investigated the behavior of the simplified FK model with parameter values that reproduce the restitution curve of the full LR model. Again, with a maximum thickness of 12 mm and a rotation rate of $24°/$mm studied, no breakup of the vortex occurred.

There are several possible explanations for the dramatic difference between the BR and LR models. First, it is possible that the twist within a filament in the LR model is distributed more homogeneously. However, our calculations show that, as is the case in the BR model, the twist is not homogeneously distributed. Second, the LR model could support more twist and therefore will not break up. To prove or disprove this possibility one would need an algorithm that can accurately calculate the filament position and its twists. We plan to address this possibility in future work. Third, it could be that collisions with the wall are occurring frequently in the LR model but fail to create an additional filament. However, our simulations show that such collisions are much rarer than in the BR model.

Finally, for a given thickness and rotation rate a filament in the LR model might not build up as much twist as a filament in the BR model. We will argue that this might be due to the difference in the spiral tip trajectories in the BR and LR models. In Fig. 3 we showed the tip trajectories for both models in homogeneous isotropic tissue and found that there are marked differences between the path taken by a
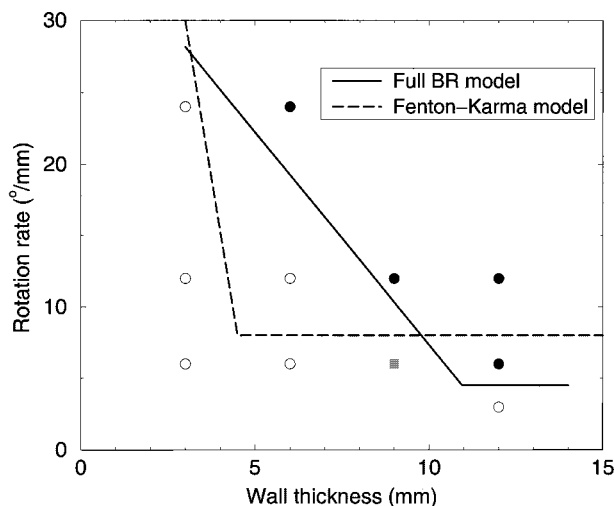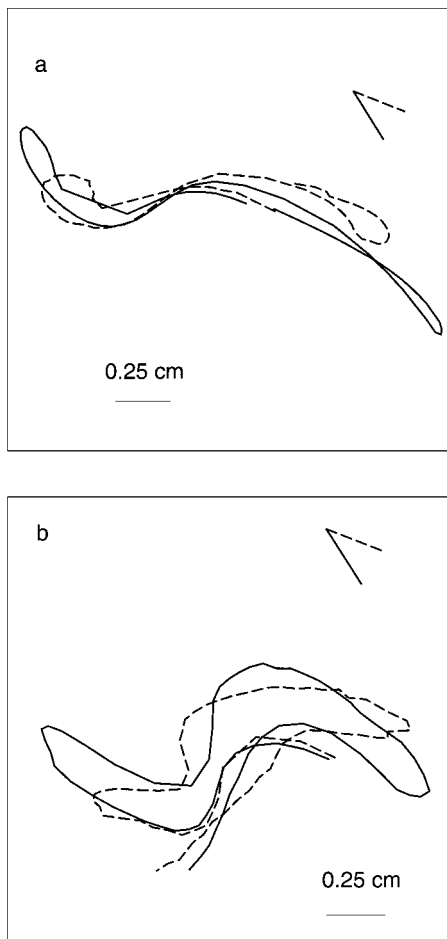

FIG. 8. A summary of our results for the BR model. Closed circles represent a final state consisting of irregular, fibrillatorylike behavior. Open circles correspond to filament that remains stable while the square represents a state in which occasional but nonsustained irregular activity occurred. The solid line marks the boundary between stable and unstable filament dynamics in the full BR model while the dashed line marks this boundary for the FK model (see Fig. 20, Ref. 7).

FIG. 9. The tip trajectory on the endocardium (solid line) and the epicardium (dashed line) for the BR model (a) and the LR model (b) for $L_z = 3$ mm and $\gamma = 12°$/mm. The trajectories represent 160 ms. The fiber angle rotations on the endocardium (solid line) and epicardium (dashed line) are displayed in the upper right-hand corner.
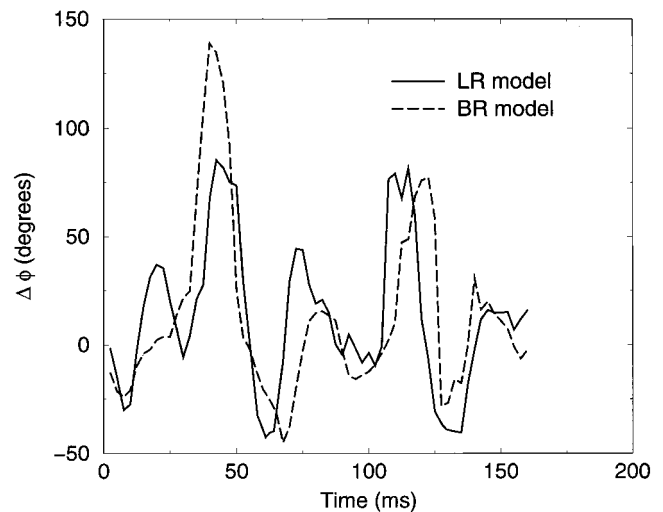

FIG. 10. The twist angle $\Delta\phi$ defined as the angle between the normals on the endo- and epicardium for the LR model (solid line) and the BR model (dashed line) corresponding to Fig. 9. Time is set arbitrarily to 0 at the beginning.

spiral tip in the BR model and in the LR model. The tip trajectory in the BR model shows pronounced petals where the trajectory makes a loop and crosses its own path. The trajectory in the LR model, on the other hand, does not exhibit these petals. Further illustration of this difference is given in Fig. 9, which shows the tip trajectory during 160 ms on the endocardium (solid line) and epicardium (dashed line) for the BR model (a) and the LR model (b). As in Fig. 3, the BR model displays turns that are rounder and the tip trajectory typically crosses its own path after a turn. As was also pointed out by FK (see Fig. 11 in Ref. 7), asynchronous turning is the primary mechanism for twist buildup in the filaments. Since a turn in the BR model involves a rotation of the normal, defined as $\hat{n} = \nabla V / |\nabla V|$, over a larger angle it is reasonable to expect a larger buildup of twist in this model. This is demonstrated in Fig. 10, which shows the twist angle, defined as the angle between the normals on the endo- and epicardium. It can be seen that the twist angle, which is a measure of the total twist within the filament, is larger in the BR model than in the LR model. A final demonstration of the importance in tip trajectories in the generation of twist and subsequent filament breakup is shown in Figs. 11 and 12. In Fig. 11 we have plotted the trajectories representing

150 ms on the endo- and epicardium for a slab with $L_z = 9$ mm and $\gamma = 12°$/mm. For the points marked $A-E$, which are 25 ms apart, we have also plotted the filament in Fig. 12. Between A and B the trajectory on the endocardium undergoes a rapid turn after which it crosses its own path. The path on the epicardium, on the other hand, does not exhibit a turn during this part of the trajectory. Consequently, a large amount of twist is built up. This is manifested clearly in Fig. 12(b) which shows that the filaments start to curve significantly starting at the endocardium. The curved portion travels along the filament and eventually hits the epicardium (frame F in Fig. 12). At this point, the filament breaks and creates multiple filaments.

VII. CONCLUSION

The main result of our numerical investigations is that rotational anisotropy in the BR model can destabilize a vortex filament and can lead to highly irregular electrical activ-
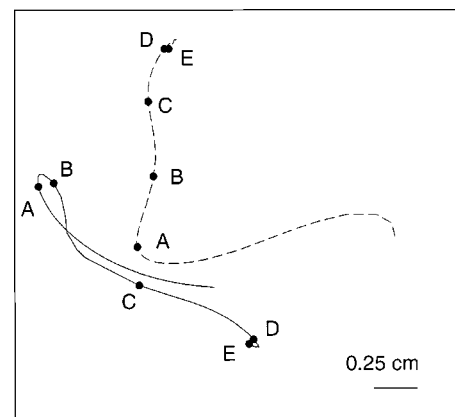

FIG. 11. The trajectory of spiral tips on the epicardium (solid line) and endocardium in the BR model for $L_z = 9$ mm and $\gamma = 12°$/mm. The total time displayed is 150 ms. The points A–E are spaced 25 ms apart and the corresponding filament at these instances in time are shown in the Fig. 12.
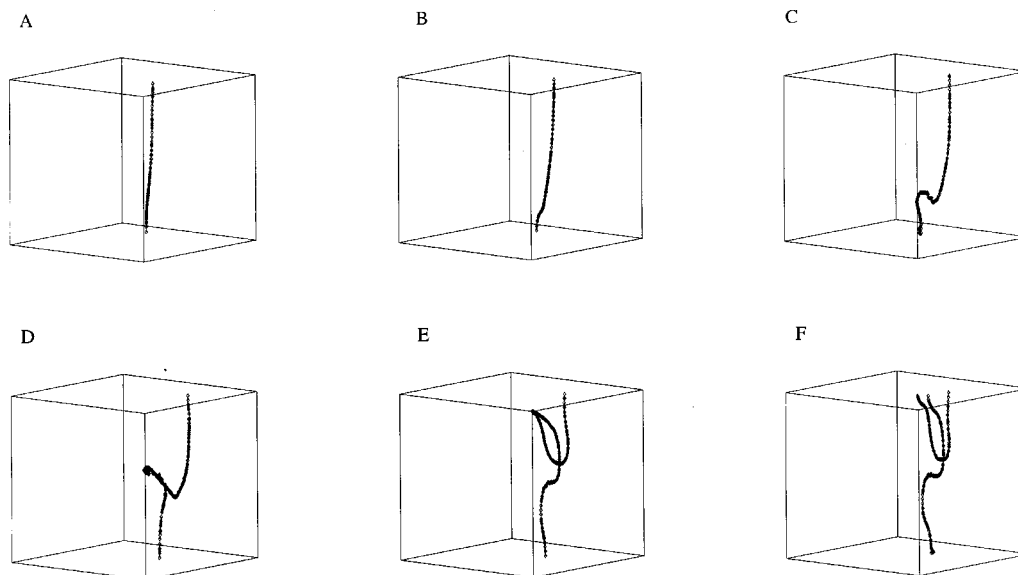
FIG. 12. The filaments corresponding to points A–E in Fig. 11 and the filament just after the collision of the curved part with the epicardium.

ity while the inclusion of rotational anisotropy in the LR model does not lead to a vortex instability. Thus, the occurrence of anisotropy-induced instabilities is model dependent. We have presented evidence that the deciding factor in the destabilization of filaments can be the spiral tip trajectory in the model. It is this trajectory that primarily determines the amount of twist that will be built up in the filament.

At present, there is no theory for spiral tip trajectories and it is unclear which factors and parameters determine the tip trajectory. One parameter that is known to play an important role is the sodium conductance, and therefore the excitability. In the BR model it was demonstrated that as the sodium conductance, and excitability, is decreased, there is a transition from a linear core to a circular core[29] (see also Fig. 7 in Ref. 7). Consistent with the observations in Ref. 7 we found that lowering the sodium conductance in the BR model has a stabilizing effect. For example, reducing the sodium conductance from $g_{Na} = 4$ mS/cm^2 to $g_{Na} = 2$ mS/cm^2 eliminated filament breakup in a slab with $L_z = 9$ mm and $\gamma = 12°$/mm. It should be noted that for this range of sodium conductances the restitution curves for the BR model remain very steep. This suggests that the restitution curves, even though they are very different in the BR and LR models, do not determine filament stability. The precise factors that determine the tip trajectory will be the subject of future research.

It is difficult to visualize spirals experimentally, even with recent advances in optical mapping techniques. The limited life span of spirals in tissue preparations further complicates matters.[17] Consequently, a precise tracking of the spiral tip has been proven to be arduous. Nevertheless, a variety of possible trajectories including inward or outward petals[17] and elliptical and linear cores[16,30] have been observed. It appears as if the spiral tip trajectory of the LR model is closer to the experimentally observed ones as is the BR model. This would suggest that rotational anisotropy is not a dominant mechanism for filament destabilization. Other possible mechanisms, including intrinsically present heterogeneities such as the presence of M cells in the healthy midmyocardium,[31] could be more important in breaking up filaments.

ACKNOWLEDGMENTS

[1] For a review, see Chaos **8**(1) (1998), focus issue on ''Fibrillation in Normal Ventricular Myocardium.''

[2] D. M. Roden *et al.*, Circulation **94**, 1996 (1996).

[3] G. K. Moe, W. C. Rheinholdt, and J. A. Abildskov, Am. Heart J. **67**, 200 (1964).

[4] A. V. Panfilov, Chaos **8**, 57 (1998).

[5] R. A. Gray *et al.*, Science **270**, 1222 (1995).

[6] A. V. Panfilov and J. P. Keener, Physica D **84**, 545 (1995).

[7] F. Fenton and A. Karma, Chaos **8**, 20 (1998).

[8] F. Fenton and A. Karma, Phys. Rev. Lett. **81**, 481 (1998).

[9] G. W. Beeler and H. Reuter, J. Physiol. (London) **268**, 177 (1977).

[10] C. H. Luo and Y. Rudy, Circ. Res. **68**, 1501 (1991).

[11] I. J. LeGrice, B. H. Smaill, L. Z. Chai, S. G. Edgar, J. B. Gavin, and P. J. Hunter, Am. J. Physiol. **269**, H571 (1995).

[12] K. D. Costa *et al.*, Am. J. Physiol. **273**, H1968 (1997).

[13] D. Streeter, in *Handbook of Physiology*, edited by R. Berne (American Physiological Society, Bethesda, 1979), Vol. 1, Sec. 2, pp. 61–112.

[14] A. T. Winfree, Chaos **1**, 303 (1991).

[15] M. A. Allessie, F. I. M. Bonke, and F. J. G. Schopman, Circ. Res. **33**, 54 (1973).

[16] J. M. Davidenko *et al.*, Nature (London) **355**, 349 (1992).

[17] D. Kim *et al.*, Chaos **8**, 137 (1998).

[18] M. Bar and M. Eiswirth, Phys. Rev. E **48**, R1635 (1993); A. Karma, Phys. Rev. Lett. **71**, 1103 (1993); A. Garfinkel *et al.*, J. Clin. Invest. **99**, 1 (1997).

[19] K. M. Kavanagh *et al.*, Circulation **85**, 680 (1992).

[20] M. A. Allessie *et al.*, Eur. Heart J. **10**, 2 (1989).

[21] A. T. Winfree, Science **266**, 1003 (1994); *Computational Biology of the Heart*, edited by A. Panfilov and A. Holden (Wiley, New York, 1997), pp. 101–135.

[22] C. H. Luo and Y. Rudy, Circ. Res. **74**, 1071 (1994).

[23] R. L. Winslow *et al.*, Circ. Res. **84**, 571 (1999).

[24] J. J. Fox (private communication).

[25] A. L. Hodgkin and A. F. Huxley, J. Physiol. (London) **117**, 500 (1952).

[26] A. Xu and M. R. Guevara, Chaos **8**, 157 (1998).

[27] M. Courtemanche, Chaos **6**, 579 (1996).

[28] H. Zhang, R. W. Winslow, and A. V. Holden, J. Theor. Biol. **191**, 279 (1998).

[29] I. Efimov, V. Krinsky, and J. Jalife, Chaos Solitons Fractals **5**, 513 (1995).

[30] S. Dillon, P. Ursell, and A. Wit, Circulation **72**, 1116 (1985).

[31] S. Sicouri and C. Antzelevitch, Circ. Res. **68**, 1729 (1991).